11-3-2020

Mass and Number Size Distributions of rBC in Snow and Firn Samples From Pine Island Glacier, West Antarctica

Luciano Marquetto

Susan Kaspari

Jefferson Cardia Simões

Earth and Space Science

RESEARCH ARTICLE
10.1029/2020EA001198

Mass and Number Size Distributions of rBC in Snow and Firn Samples From Pine Island Glacier, West Antarctica

Luciano Marquetto[1,2], Susan Kaspari[1], and Jefferson Cardia Simões[2,3]

[1]Department of Geological Sciences, Central Washington University, Ellensburg, WA, USA, [2]Centro Polar e Climático, Universidade Federal do Rio Grande do Sul, Porto Alegre, Brazil, [3]Climate Change Institute, University of Maine, Orono, ME, USA

Key Points:
- First detailed rBC mass and number size distributions from snow and firn from West Antarctica
- rBC mass size distributions are polymodal with a primary mode at 162 nm and other modes at 673, 1,040, and an uncontained mode >1,810 nm
- rBC particles (particularly those smaller than 500 nm) are depleted in the wet season compared to the dry season

Supporting Information:
- Supporting Information S1

Correspondence to:
L. Marquetto,
luciano.marquetto@gmail.com

Citation:
Marquetto, L., Kaspari, S., & Simões, J. C. (2020). Mass and number size distributions of rBC in snow and firn samples from Pine Island Glacier, West Antarctica. *Earth and Space Science*, *7*, e2020EA001198. https://doi.org/10.1029/2020EA001198

Received 23 APR 2020
Accepted 18 OCT 2020
Accepted article online 3 NOV 2020

Abstract An extended-range Single Particle Soot Photometer (SP2) coupled to a Marin-5 nebulizer was used to measure the refractory black carbon (rBC) mass and number size distributions in 1,004 samples from a West Antarctica snow/firn core. The SP2 was calibrated using Aquadag and a Centrifugal Particle Mass Analyzer for BC particles ranging from 0.5 to 800 fg. Our results indicate a significant contribution of rare, large particles of mass-equivalent diameter (D_{BC}) > 500 nm to the total rBC mass (36%), while small particles (D_{BC} < 100 nm) are abundant but contribute <8% to total rBC mass. We observed a primary mass median diameter of 162 ± 40 nm, smaller than reported for snow in other regions of the globe but similar to East Antarctica rBC size distributions. In addition, we observed other modes at 673, 1,040, and >1,810 nm (uncontained mode). We compared two sets of samples from different seasons (wet vs. dry) and observed that dry season concentrations are 3.4 and 2 times that of the wet season in the ranges of 80 nm < D_{BC} < 500 nm (small particles) and 500 nm < D_{BC} < 2,000 nm (large particles), respectively, while number of particles in the dry season is 3.5 and 2 times that of the wet season for the same size ranges. Millimeter thick melt layers have been observed in some samples, although they did not change the observed median diameter. This study provides the first detailed rBC mass and number size distribution from West Antarctica.

Plain Language Summary Black carbon (BC) is a particle produced by the incomplete combustion of biomass burning and fossil fuels and plays an important role in the climate system due to its strong light absorption properties. The size of BC particles in snow is important for determining the effects that BC has on the cryosphere and provides insight into the processes controlling BC emission history, transport, and deposition. Past studies indicate spatial differences of BC size distributions in snow, but these studies are limited in number, and more are needed to address this spatial variability. Here the size distribution is presented of BC particles from 1,004 samples from a Pine Island Glacier ice core, West Antarctica, in a region where there is no information of BC particle size in snow. BC in West Antarctica is smaller than other regions of the globe but large, rare particles are also present. These large BC particles are larger than what other studies have reported and could be a result of long-range transport from other continents and/or agglomeration from small particles during transport or deposition.

1. Introduction

Black carbon (BC) is a carbonaceous aerosol emitted by incomplete combustion of fossil fuels and biomass that affects the climate due to its strong light-absorption properties (Goldberg, 1985; IPCC, 2013). BC absorbs the most solar light per unit mass of any atmospheric aerosol (Schwarz et al., 2013) and, when deposited on snow and ice, reduces albedo and accelerates melt (Bond et al., 2013; Hadley & Kirchstetter, 2012). Increases in BC concentrations since the industrial revolution have been observed in ice sheets and glaciers around the world (McConnell et al., 2007; Osmont et al., 2019; Thevenon et al., 2009), with direct implications to the planetary albedo (Bice et al., 2009; Bond et al., 2013; Hansen & Nazarenko, 2004).

The impact of BC on snow albedo depends on a number of factors, including BC content in snow (He et al., 2018), mixtures with other particles (Warren & Wiscombe, 1980), and BC particle properties. BC size is a significant source of uncertainty when estimating BC absorption properties in snow (Schwarz et al., 2013). These authors state there is a possible overestimation of BC global mean snow forcing up to 30% as

atmospheric BC size distributions, rather than snow BC size distributions, are used to model BC impacts in the cryosphere.

The Single Particle Soot Photometer (SP2) is a useful method to address these uncertainties, as the technique is able to provide size distributions of BC in the atmosphere and snow. The SP2 measures thermal radiation emitted by laser-induced incandescence of individual BC particles (reported as refractory black carbon—rBC, as recommended by Petzold et al., 2013). The rBC size distributions are commonly presented in mass and number (or count) distributions, and by fitting a lognormal function to them, it is possible to obtain the mass median diameter (MMD) and number median diameter (NMD) of the distributions, respectively.

Previous studies have shown rBC size distribution in the atmosphere tends to follow a pure lognormal function, with an MMD of ~220 nm or smaller and less than 1% of total mass associated with particles of mass equivalent diameter (D_{BC}) > 600 nm (Schwarz et al., 2013). Urban atmosphere rBC MMD tends towards lower medians (~100 nm), while remote atmosphere rBC MMD presents higher values (~220 nm—Schwarz et al., 2012, 2013), although the opposite has also been reported (Wu et al., 2017, and references therein).

The size distribution of rBC in snow presents an MMD similar to remote atmospheric sites (~220 nm—Lim et al., 2014; Schwarz et al., 2013) but deviates from a lognormal distribution due to the contribution of particles with D_{BC} > 500 nm. Schwarz et al. (2013) found that particles with D_{BC} > 600 nm represented 28% of the rBC mass in snow samples from rural and semirural Colorado, USA. This is an important observation, as BC absorption properties differ with particle size. When BC diameter is small relative to the light's wavelength, the particle absorbs light proportionally to its mass. However at larger sizes, light absorption is proportional to particle surface area (Schwarz et al., 2013).

In Antarctica, the literature about BC size distributions is still scarce; thus, more observations are needed. The most extensive work was carried out by Kinase et al. (2019) for East Antarctica around Syowa Station. The authors found a bimodal distribution in BC in snow, with MMDs of ~140 and 690 nm and NMDs around 70 nm; postdepositional processes affected BC concentrations but not size distributions. Khan et al. (2018) presented rBC volume distributions (rather than MMD) showing large rBC particles of 300–400 nm in a shallow snow pit in McMurdo Dry Valleys. Ellis et al. (2016) observed a substantial fraction of small particles (D_{BC} < 90 nm) in East Antarctica snow and ice, although only qualitatively. Thus, further studies of Antarctic BC mass size distributions are necessary. Furthermore, as BC is mainly deposited in snow through wet deposition (Flanner et al., 2007), measuring the size distribution of BC particles in snow should improve our quantitative understanding of the BC wet removal mechanism from the atmosphere (Mori et al., 2016).

In this work we present the rBC number and mass size distributions of 1,004 snow samples from a 20 m snow/firn core (TT07) drilled in West Antarctica during the 2014/2015 austral summer that spans 1968–2015 (Marquetto, Kaspari, & Simões, 2020). The rBC present in the core likely reflects long-range transport from sources in South America and Australia/New Zealand and is associated mostly with biomass burning emissions (Arienzo et al., 2017; Bisiaux, Edwards, McConnell, Albert, et al., 2012; Koch et al., 2007; Stohl & Sodemann, 2010).

2. Site Description and Field Campaign

The core presented in this study (TT07) was drilled on the Pine Island Glacier at 79°55′34.6″S, 94°21′13.3″W (elevation 2,122 m a.s.l.), near the Mount Johns Nunatak (located 70 km NE of the drilling site) (Figure 1).

The core was retrieved in 21 sections of less than 1 m each, weighed in the field, packed in polyethylene bags, and then stored in high-density Styrofoam boxes. Borehole temperature measured in the field was −34°C at 12 m deep. We used a probe previously calibrated that remained in the borehole for at least 8 hours. The core was sent by air to Punta Arenas (Chile), then to a deposit in Bangor (USA) for storage and finally to the Central Washington University Ice Core Laboratory (Ellensburg, WA), where it was kept at −18°C in a clean cold room until subsampling and analysis. During transport between Antarctica and Bangor the core was exposed to above-freezing temperatures, and some sections were partially melted and refrozen. As the core was transported lying down in the boxes, this melt and refreeze occurred in the external part of the core and

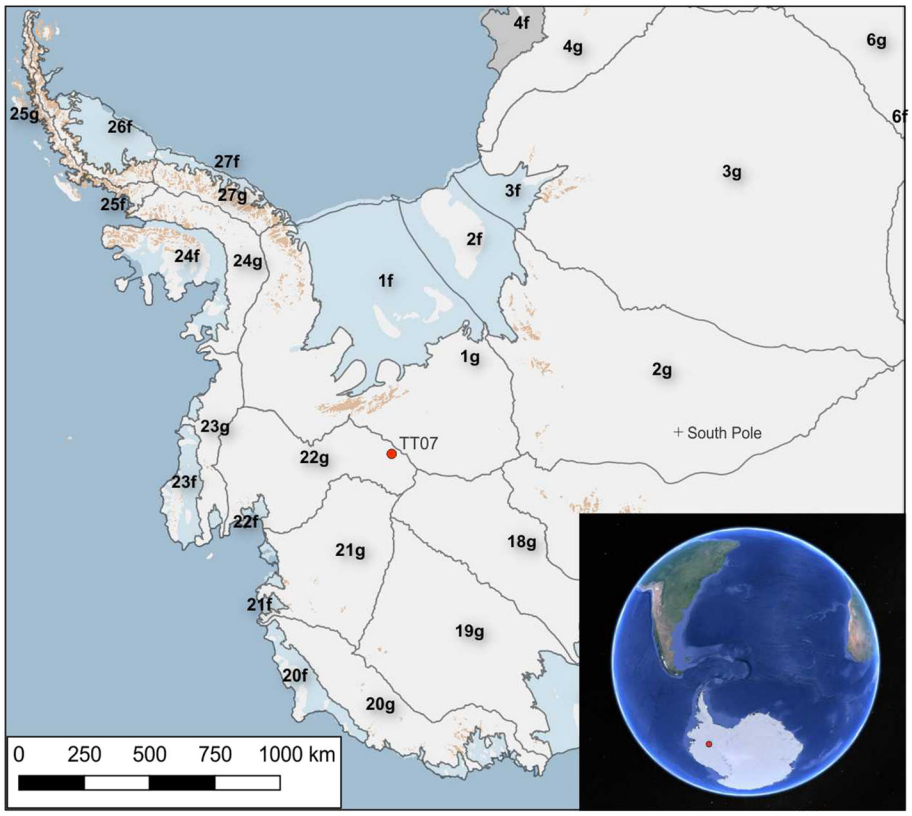

Figure 1. Drilling location for the snow/firn core analyzed in this work (TT07). Black lines show West Antarctic ice divides (1 g = Institute Glacier; 22 g = Pine Island Glacier). Data from BEDMAP 2 project (Fretwell et al., 2013). The bottom right shows the drilling site relative to South America.

did not reach the center of it. The melted and refrozen portion of the core was removed by saw and hand scraping, and only a small 10-cm piece of section 07 was discarded as it was totally refrozen.

3. Materials and Methods

3.1. General Information on the SP2

We used an extended range SP2 coupled to a Marin-5 nebulizer (Teledyne CETAC Technologies, Omaha, NE, USA), in the Department of Geological Sciences, Central Washington University (CWU), WA, USA to analyze the snow and firn samples.The SP2 (Droplet Measurement Technologies—DMT, Boulder, CO, USA) is widely applied in aerosol science and is one of the most reliable instruments to analyze BC on a particle-by-particle basis (Wendl et al., 2014). It was adapted to analyze meltwater of snow and ice samples by McConnell et al. (2007), and since then it has been extensively used to analyze seasonal snow (e.g., Delaney et al., 2015; Schwarz et al., 2012), high-altitude glacier surface snow and ice cores (e.g., Kaspari et al., 2011, 2014; Lim et al., 2017; Osmont et al., 2019; Sigl et al., 2018), and polar snow and ice (e.g., Arienzo et al., 2017; Bisiaux, Edwards, McConnell, Albert, et al., 2012; Bisiaux, Edwards, McConnell, Curran, et al., 2012; Casey et al., 2017). The SP2 uses laser-induced incandescence to measure the rBC mass of individual particles as the peak intensity of light that a particle emits is proportional to its size and mass (Schwarz et al., 2006; Slowik et al., 2007). The SP2 rBC measurement is negligibly affected by other materials (Moteki & Kondo, 2010; Schwarz et al., 2006, 2012).

These characteristics allow the SP2 to reconstruct accumulation-mode size distributions of rBC from samples (Schwarz et al., 2010), as the indirect mass measurement can be then converted to size using the equation:

$$D_{BC} = \left(\frac{6\,M}{\pi\,\rho_{true}}\right)^{1/3} \quad (1)$$

where D_{BC} is the rBC particle mass equivalent diameter, M is the particle mass, and ρ_{true} is the true density of the particle considered (commonly assumed to be 1.8 g cm^{-3}; Moteki & Kondo, 2010). Mass equivalent diameter is also presented in the literature as D_{MEV} (Cheng et al., 2018).

The standard SP2 detects particles in the 70–500 nm mass-equivalent diameter (D_{BC}) range (DMT, 2013b), but CWU has an extended-range SP2, capable of detecting particles between 80 and 2,000 nm D_{BC} (assuming a BC density of 1.8 g cm^{-3}). For details of the extended range SP2, see Mori et al. (2016) and Moteki and Kondo (2010).

Data processing was performed with the SP2 Toolkit 4.200 developed by the Laboratory of Atmospheric Chemistry at Paul Scherer Institute (PSI) and was used on the scientific data analysis software IGOR Pro versions 6.3 and 7. Data are reported as rBC, following recommendations from Petzold et al. (2013).

3.2. Sample Preparation

Details on laboratory and cold room cleaning as well as the cut plan for the samples are presented in Marquetto, Kaspari, Simões, and Babik (2020). Briefly, the samples were hand scraped with a clean ceramic knife in a laminar flow hood inside a cold room, to remove the outer snow/firn layer (2–4 mm). They were stored in precleaned 50-mL polypropylene vials and kept frozen until analysis. Just prior to analysis, the samples were melted at room temperature or in a warm bath (not exceeding 25°C) and sonicated for 15 minutes prior to analysis. Most samples were analyzed in less than 30 minutes after melting, and all samples were analyzed in less than 2 hours after melting.

3.3. Sample Nebulization

As the SP2 was initially designed to analyze BC from the atmosphere (dry aerosol), it is necessary to nebulize the sample before it enters the SP2 inlet. For this step, we used a CETAC Marin-5 nebulizer.

The nebulization step induces losses of rBC particles during the sample analysis (imperfect nebulization, removal of rBC with the drain water, and adsorption of rBC at the surface of the capillaries), meaning that only a fraction of BC particles initially pumped from the sample will reach the SP2 inlet (Katich et al., 2017). This fraction corresponds to the nebulization efficiency. Previous works have shown that the Marin-5 nebulization efficiency is not size dependent in the 200–3,000 nm diameter range (Katich et al., 2017; Mori et al., 2016). The nebulization efficiency for the Marin-5 at CWU was calculated to be 68.31% $\pm$ 5.91% (1σ) (Marquetto, Kaspari, Simões, & Babik, 2020).

In this work we assume that the melting and nebulization processes do not cause BC agglomeration that would shift the size distribution to larger sizes, based on the same assumptions as Schwarz et al. (2013). We also assume that the sonication process did not alter the mass or number size distribution of samples, based on results obtained by Mori et al. (2014) for 25 rainwater samples analyzed for rBC in the 70–850 nm detection range. The Marin-5 and SP2 were arranged to minimize bends in the conductive silicon tubing transport line, with one bend in the SP2 inlet. We consider the mass size distribution curve obtained by the SP2 to represent the original rBC size distribution of the snow samples. Our results may have been affected by transport losses of aerosols, which increase quickly with increasing size above 1,000 nm (personal communication with J. Schwarz); however, this was not assessed in this work.

3.4. SP2 Calibration

The SP2 needs empirical calibration to assign a BC mass to a given SP2 response, referred to as internal calibration by Wendl et al. (2014). The internal calibration is obtained by recording the average incandescent signal peak height for pure BC particles of a known mass over the whole dynamic range of the SP2 (Gysel et al., 2011). An additional calibration, called external calibration, is necessary when analyzing liquid samples to correct for BC losses during the nebulization process.

The internal calibration was carried out on CWU's SP2 using a Centrifugal Particle Mass Analyzer (CPMA) to mass-select BC particles of a known polydisperse BC standard consisting of Aquadag (Acheson Industries Inc., Port Huron, MI, USA) diluted in Milli-Q water (MilliQ-Element, Millipore, Milford, USA; 18.2 M Ω).

Aquadag was also used for the daily SP2 external calibration (details of the external calibration are in Marquetto, Kaspari, Simões, & Babik, 2020).The use of a CPMA to mass-select BC particles in the SP2 internal calibration is recommended in Schwarz et al. (2012) to reduce uncertainties associated with detection of large rBC particles. Particle mass analyzers select particles by their mass-to-charge ratio by balancing electrostatic and centrifugal forces and are a better choice for particle calibration than Differential Mobility Analyzers (DMA) as the latter classifies particles by size and thus needs further corrections along with BC density assumptions in order to calculate the particle mass (Gysel et al., 2011; Olfert & Collings, 2005). Also, the CPMA has an uncertainty of only 1.4% in mass measurements for single-charge particle (Symonds et al., 2013). Even though the use of a CPMA reduces the uncertainty associated with large rBC particles, there are uncertainties related to the behavior of Aquadag at very large masses, due to the unknown morphology of the rBC in the snow/ice (personal communication with J. Schwarz). These uncertainties are beyond our scope and are not addressed in this work.

We configured the CPMA to select 23 particle masses from 0.5 to 800 fg (translating to D_{BC} ~ 80–1,000 nm); each mass was measured for 30 minutes to 6 hours to provide statistically significant particle triggers to calibrate the SP2. Most literature about BC in snow and ice used a DMA for calibration and ran up to particle sizes equivalent to 100 fg (Katich et al., 2017; Lim et al., 2014; Osmont et al., 2018; Schwarz et al., 2012); some extended further (Lim et al., 2017—220 fg; Mori et al., 2016—300 fg). Moteki and Kondo (2010) extended their calibration up to 400 fg with Aquadag and to 800 fg with Glassy Carbon (although the later consists of >400 nm spherical, compact particles, different from ambient soot). To our knowledge, no calibration as broad as this work (0.5–800 fg) using a CPMA is documented in the literature.

Extrapolations of the calibration limits (80–1,000 nm) to the full detection limits of the CWU SP2 (80–2,000 nm) were made based on the relationship between particle mass and incandescent signal. Moteki and Kondo (2010) observed that for small particles ($M < 10$ fg) the incandescent signal is linearly proportional to particle mass, while the relationship for larger particles (10 fg $< M <$ 800 fg) is dependent on particle shape and calculated using an empirical power law. These observations, though, were made using a DMA for the SP2 internal calibration. In the internal calibration carried out in this work we observed that the polynomial splines (least squares fit) from the PSI SP2 toolkit presented the best fit both in the lower and higher end of the SP2 detection range, so we used these for extrapolation. We note that between 1,000 and 2,000 nm void free diameter the calibration is extrapolated by a factor of 8. When necessary to adjust the curvature of the calibration curve at the low end, the fits were adjusted by segments as described in DMT (2013a). The power law and the linear fit from Moteki and Kondo (2010) do not agree with our calibration data as well as the polynomial splines in the lower and higher end of the calibrated ranges (Figures 2a–2c).

The use of Aquadag for the SP2 internal and external calibrations is described in the literature (Gysel et al., 2011; Moteki & Kondo, 2010). We utilized Aquadag because the SP2 sensitivity to its BC-type is known, and its mass-size distribution most closely represents the mass size distributions observed in snow: ~100–1,000 nm (Wendl et al., 2014). Regarding particle morphology, Aquadag is characterized by fluffy aggregates of thin flakes and small spherules of crystalline graphite (Moteki et al., 2009), similar to non-compact ambient soot (Moteki & Kondo, 2010). A scaling factor of 0.75 was applied for the external calibration carried out in this work, which accounts for the non-BC mass in Aquadag. Baumgardner et al. (2012) indicate that internal calibrations done with Aquadag should also be scaled downwards by a factor of 0.75, as the SP2 is 23–29% less sensitive to fullerene soot, the recommended reference material for atmospheric calibrations, than to Aquadag. These different sensitivities represent about a 10% shift in volume-equivalent diameter when comparing uncorrected and corrected calibrations. However, we opted to keep our internal calibration uncorrected because the signal ratio of BC from ice cores and snow samples sometimes resembles that of fullerene soot, sometimes that of Aquadag (Wendl et al., 2014, supporting information) and might more often resemble that of the latter (M. Gysel, personal communication).

The data presented in this work were obtained from the duplicated extended range broadband detector of the SP2 (the combination of the high gain and low gain amplifications: B2HG + B2LG). These channels presented the best fit calibration curve of all channels, with a precise fitting in the lower (B2HG) and higher (B2LG) end of the particle mass range (calibration curves in Figure 2). The B2HG channel was able to detect particles in the 80–600 nm size range, while the B2LG detection range was 80–2,000 nm. As expected from

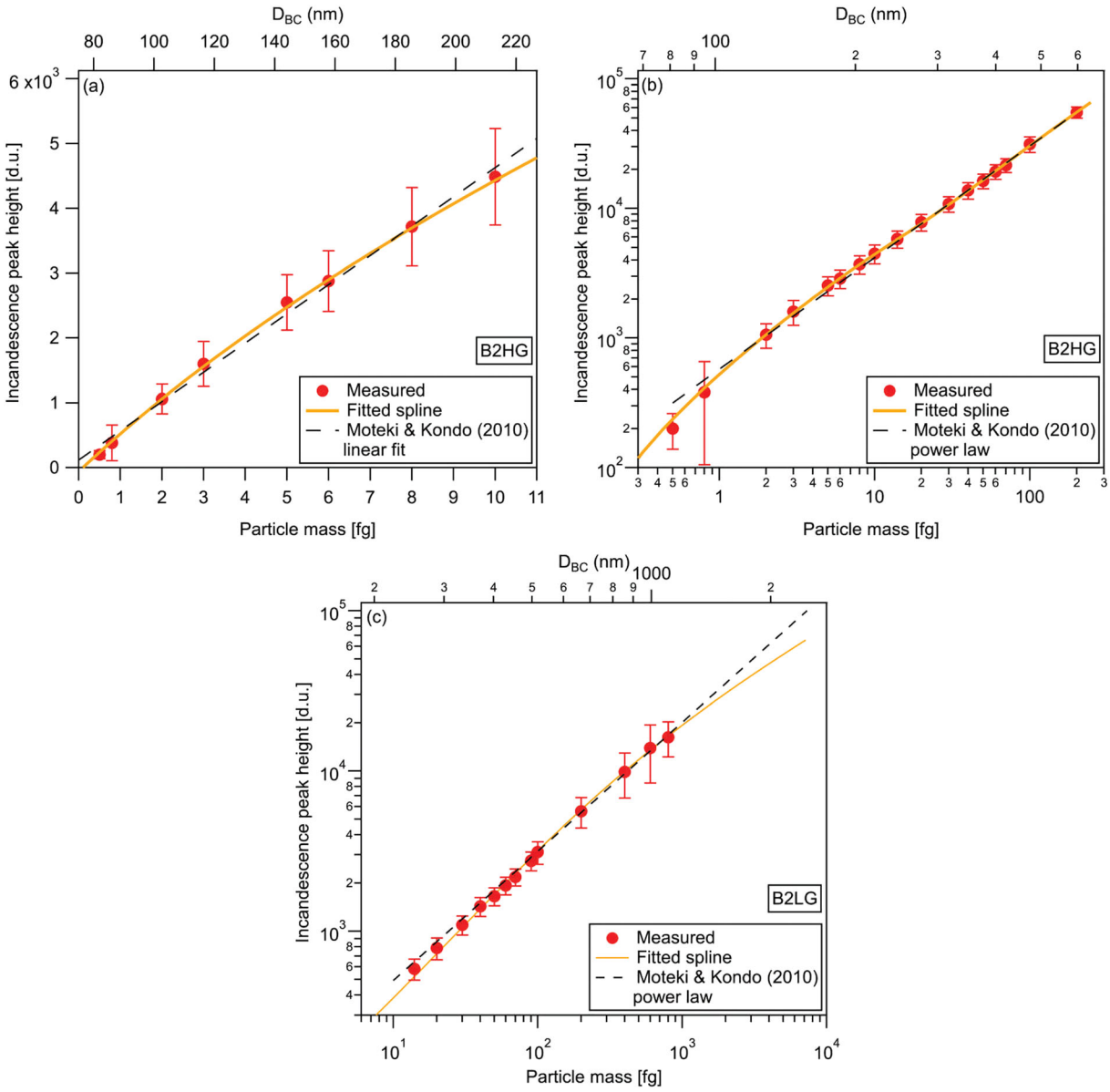

Figure 2. Calibration curves for the (a) B2HG channel ($0.5 < M < 10$ fg—linear scale), (b) B2HG channel ($0.5 < M < 200$ fg—logarithmic scale), and (c) B2LG channel ($14 < M < 800$ fg—logarithmic scale), obtained from the internal calibration carried out using the SP2 + CPMA. The B2HG channel showed a good fit for low mass particles (0.5–200 fg), while the B2LG channel presented a good fit for larger particles (200–800 fg). Also shown for comparison are the measured relationships from Moteki and Kondo (2010)—linear fit for $M < 10$ fg and power law for $20 < M < 800$ fg. Incandescence peak height is presented in (arbitrary) defined units (d.u.). Particle size was calculated using the formula presented in section 3.1, assuming ρ_{true} as 1.8 g cm^{-3}. Error bars represent one standard deviation of mean peak height (Table S1presents more results of calibration time, particle triggers, and mean peak height ± standard deviation for each calibration mass).

previous works (Mori et al., 2016; Moteki & Kondo, 2010), the incandescence peak height observed in the internal calibration for larger particles is not linearly correlated to their mass as particle effective density (ρ_{eff}) is $\neq 0$. ρ_{eff} is a measure of the compactness of the particle shape and can vary from zero for extremely non-compact particles (highly branched aggregates), up to the true density (~1.8 g cm^{-3}) for extremely compact particles (spherical) (Moteki & Kondo, 2010).

3.5. Sample Grouping and Seasonal Classification

To achieve a statistically significant rBC size distribution it is necessary to collect a large number of rBC particles in the SP2. Katich et al. (2017) empirically determined this number to be ~40,000 particles for typical

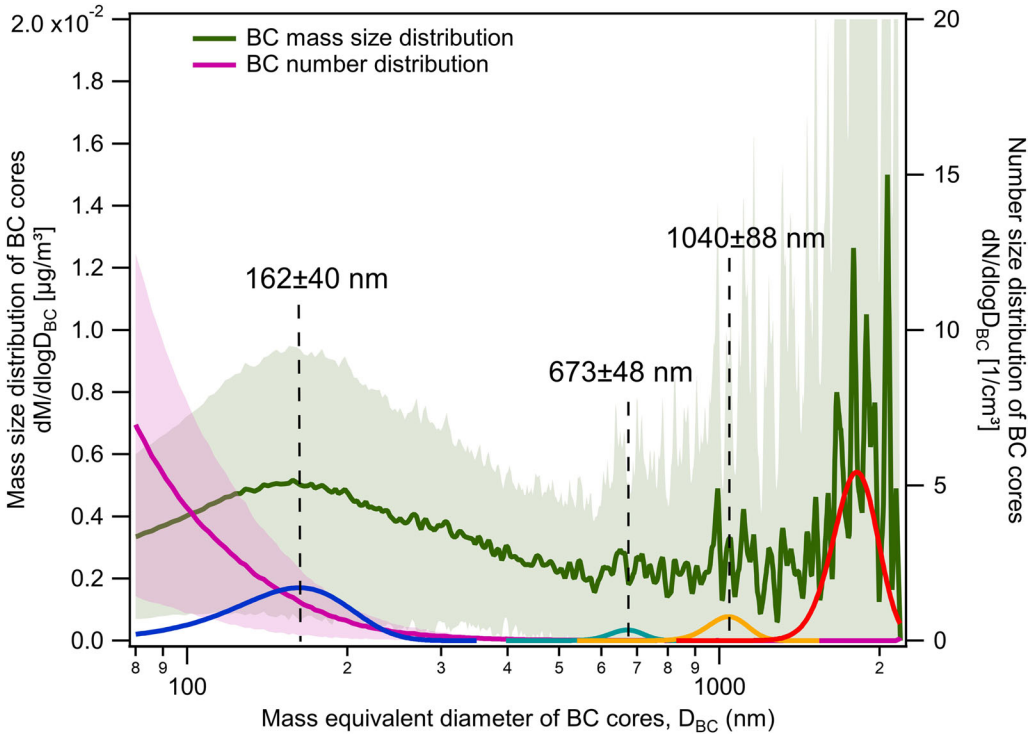

Figure 3. Mass and number size distributions for the full set of samples. Shaded areas represent one standard deviation (68.3%) of the number distribution (shaded purple) and mass distribution (shaded gray). Gaussian fits are shown for the mass size distributions at the bottom of the graph. The larger mode at ~1,810 nm is not fully characterized and may extend further than 2,000 nm. Standard deviation for D_{BC} > 1,500 nm (up to 2.5 times the scale) not shown.

ambient snow, although this number could be much higher if rare, large rBC particles are present in the sample, as these could change the size distribution towards larger values.

Considering the low BC concentration in the samples, especially in the wet season (as low as 200 detected particles/sample), we present our results as a grouping of individual samples in 94 seasonally resolved clusters (wet season subset = summer/fall, 474 samples and 47 clusters; dry season subset = winter/spring, 530 samples and 47 clusters). The number of clusters is due to the estimated dating of the core (47 years, Marquetto, Kaspari, & Simões, 2020). Although the dry season subset presented considerably more particles ($n = 8.28 \times 10^5$) than the wet season subset ($n = 2.03 \times 10^5$), both have a robust number of collected particles.

The size distributions for the full set of samples (Figure 3) are the result of grouping and averaging the 94 clusters together, and the MMD and NMD were obtained by fitting Gaussian fits to the mass and number size distributions, respectively, using Igor Pro 7 multipeak fitting tool version 2 (noise level: 0.000190962; min fraction: 0.05; smooth factor: 10 for particles with D_{BC} < 500 nm; smooth factor 30 for particles with D_{BC} > 500 nm). Dry and wet season primary MMDs were obtained using the same tool but different parameters (dry season—noise level: 0.000190962; min fraction: 0.05; smooth factor: 10; wet season—noise level: 8.21095e-05; Min fraction: 0.05; smooth factor: 30). Standard deviation was obtained from the full width at half maximum (FWHM) of the Gaussian fits, as the standard deviation in a Gaussian fit is equal to the FWHM divided by 2.35.

Seasonal sample discrimination was based on the core dating presented in Marquetto, Kaspari, and Simões (2020). Antarctic ice core BC records show a well-defined seasonality, with peak concentrations in the dry season due to increased biomass burning activity in the Southern Hemisphere (SH) during this time of the year (Bisiaux, Edwards, McConnell, Curran, et al., 2012; Sand et al., 2017; Winstrup et al., 2019); more efficient transport to the ice core site (Marquetto, Kaspari, & Simões, 2020; Neff & Bertler, 2015; Schwanck et al., 2017; Stohl & Sodemann, 2010); and weaker precipitation (Legrand & Mayewski, 1997; Sinclair et al., 2010). The wet season is identified by much lower BC concentrations. The core presented in this

study was dated to 47 years and showed geometrical mean concentration of 0.06 μg L^{-1} for the dry season and 0.01 μg L^{-1} in the wet season (Marquetto, Kaspari, & Simões, 2020). As for BC size distribution, we considered only results in the CWU SP2 calibration range (80 nm > D_{BC} > 2,000 nm).

4. Results and Discussion

4.1. Size Distribution of rBC in the Antarctic Snow Samples

Figure 3 shows the mass and number size distributions for the full set of samples. We observed the mass size distribution presented a multimodal distribution with three MMDs at 162 ± 40, 673 ± 48, and 1,040 ± 88 nm. A larger MMD was identified at 1,810 ± 174 nm, although this larger mode is not fully characterized and is an uncontained mode that extends to masses >2,000 nm.

The number counting of BC particles (N_{BC}) indicates most particles analyzed are of very small size. Particles with D_{BC} < 100 nm were abundant (45% of the total N_{BC} between 80 and 2,000 nm) but represent only 7.4% of the total mass. Particles with D_{BC} > 500 nm, on the other hand, proved to be very rare (0.46% of the total N_{BC} between 80 and 2,000 nm) but represent 36.4% of the total rBC mass. These results indicate that large particles exist in Antarctic snow and ice and that despite their low occurrence, they can represent an important fraction of total rBC mass in the snow.As for seasonal variations (Figure 4 and Table 1), particles with D_{BC} < 100 nm represent ~48% of all rBC N_{BC} both in the dry and wet season and 8.5% (dry season) and 6.7% (wet season) of total rBC mass. The MMD for both seasons is similar to the full core, with the dry season presenting a slightly lower (160 ± 40 nm) than the wet season MMD (187 ± 31 nm). The wet season presented a lower contribution of particles in the 100 nm > D_{BC} > 500 nm to total seasonal mass than the dry season, which is observed in Figure 4a as a flatter curve. We also observed that the contribution of particles with D_{BC} > 500 nm to total rBC mass is higher in the wet season than in the dry season: 45.4% versus 33.3% and represent 0.38% and 0.21% of all rBC particles in each season, respectively. Dry season concentrations are 3.4 and 2 times that of the wet season in the ranges of 80 nm < D_{BC} < 500 nm (small particles) and 500 nm < D_{BC} < 2,000 nm (large particles), respectively; particle abundance in the dry season is 3.5 and 2 times that of the wet season for the same size ranges. The seasonal differences may indicate different rBC origins, transport, aging, or deposition processes for both seasons.

We observed millimeter thick ice layers in the core's stratigraphy, likely associated with summer melting due to solar radiation in austral summer. However, these samples are not necessarily associated with high BC concentrations, as they ranged from as low as 0.02 to 0.08 μg L^{-1}. Also, they did not present MMD differences compared to samples of similar concentrations but with no ice layers (not shown). This suggests the melting was not an important postdepositional process for rBC. This result is supported by Doherty et al. (2013) that found only very limited redistribution of BC in a snow and firn vertical profile with melt layers much thicker (>10 cm) than the ones found in TT07 (~1 mm).

4.2. Comparison With Other Studies

Figure 5a compares the rBC mass distribution observed in the Antarctic samples with previous studies in snow from different parts of the globe, and Table 2 summarizes them. Ohata et al. (2013) analyzed 20 snow samples from Sapporo, a semi urban area in northern Japan; Schwarz et al. (2013) analyzed five fallen snow samples from three snowfalls in semirural and rural areas of Denver, CO, USA; Sinha et al. (2018) analyzed 167 samples of different types (fresh snow, falling snow, and from the snowpack) from Ny-Ålesund, Spitsbergen; Mori et al. (2019) did an extensive work analyzing the size distribution of BC in 296 samples from the snowpack over Finland, Alaska, Siberia, Greenland, and Spitsbergen during early spring in 2012–2016. At last, for Antarctica, Kinase et al. (2019) analyzed the mass and size distribution of 26 snow samples collected from April to December 2011 at Syowa station (East Antarctica) and along a traverse route to an inland (Mizuho) station, and Khan et al. (2018) presented an averaged rBC volume distribution of 11 samples from a snow pit in the McMurdo Dry Valleys, West Antarctica. We do not include results from Khan et al. (2018) as rBC volume distribution differs from size distributions presented here.

The MMD of the samples analyzed in this work is similar to Kinase et al. (2019) for East Antarctica and smaller than the MMDs observed for snow in other regions of the globe. As for the number distribution, the Antarctic samples from this study presented a slightly lower but still similar NMD than other very remote regions (East Antarctic samples from Kinase et al., 2019) and Greenland samples from Mori et al. (2019),

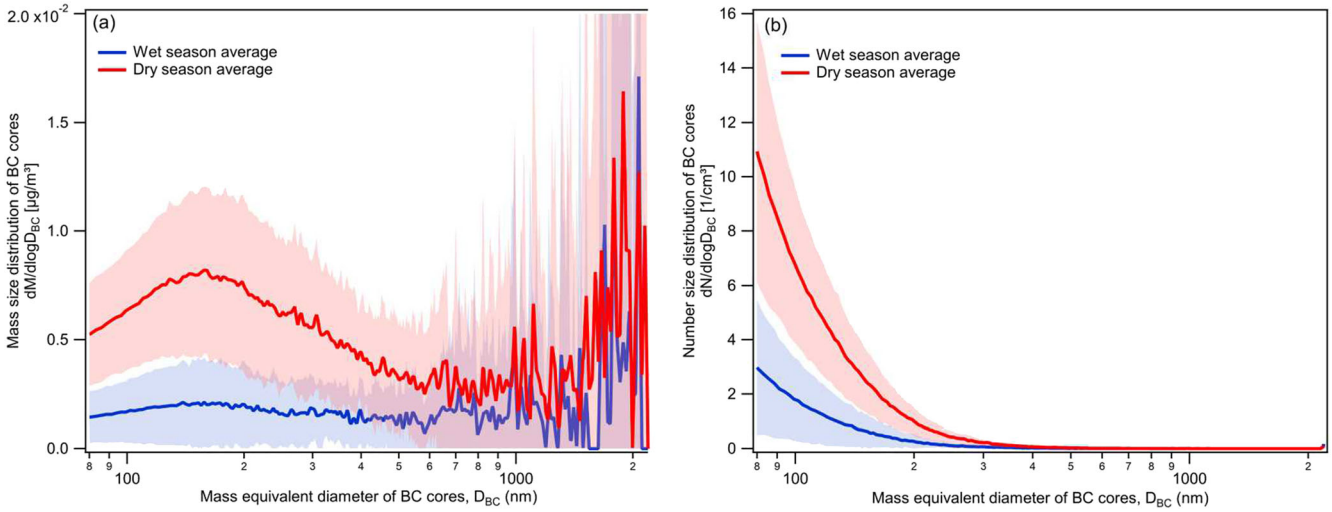

Figure 4. Mass and number size distributions for the dry ($n = 8.28 \times 10^5$ particles) and wet season ($n = 2.03 \times 10^5$ particles). Shaded areas represent one standard deviation (68.3%) of the wet (shaded blue) and dry (shaded red) seasons. Standard deviation for D_{BC} > 1,500 nm (up to 2.5 times the scale) not shown in 4a.

while differing greatly from more populated areas (Sapporo samples from Ohata et al., 2013) and Ny-Ålesund samples from Sinha et al. (2018).

While other studies have shown the contribution of particles with D_{BC} > 500 nm to total mass in snow (e.g., for the USA, Schwarz et al., 2013; Spitzbergen, Sinha et al., 2018; the Arctic, Mori et al., 2019; East Antarctica, Kinase et al., 2019; and in the [Chinese] atmosphere, Huang et al., 2011; Wang et al., 2014; and Wu et al., 2017), our results showed the highest contribution of all (Figure 5 and Table 2). The snow samples from Japan (Ohata et al., 2013), the United States (Schwarz et al., 2013), and Spitzbergen (Sinha et al., 2018) do not present a secondary mode, although particles with D_{BC} > 500 nm represent ~25% of the total mass in Spitzbergen (Sinha et al., 2018) and ~30% in the United States (Schwarz et al., 2013). The samples from East Antarctica (Kinase et al., 2019) show a secondary mode at ~690 nm, similar to this work's mode at 673 nm, and some of the Arctic samples (Mori et al., 2019) presented secondary modes around 1,200–1,400 nm, closer to the 1,040 nm found in this work.

4.3. Size Distribution Interpretation

The rBC size distribution in snow can be affected by several factors: emission type (biomass or fossil fuel burning), aging, transport, removal from the atmosphere, and postdepositional processes (Bond et al., 2013).

The formation of rBC particles is a complex process that depends on oxygen/fuel mixing states and involves a series of reactions of polycyclic aromatic hydrocarbon molecules. Different burning origins (e.g., open biomass burning and fossil fuel combustion) generate different particle morphologies, size distributions, and MMDs (Bond et al., 2013). Even the same burning origin generates BC with different characteristics as the process evolves, as happens when biomass burning changes from flaming to smoldering (Reid et al., 2005).

Table 1
Comparison Between the Full Core, Dry Season and Wet Season Number, and Mass Size Distributions

	Full core	Dry season	Wet season
MMD (primary mode)	162 ± 40 nm	160 ± 40 nm	187 ± 31 nm
NMD	<80 nm	<80 nm	<80 nm
D_{BC} < 100 nm mass	7.4%	8.5%	6.7%
D_{BC} < 100 nm number	45.4%	47.9%	48.0%
D_{BC} > 500 nm mass	36.4%	33.3%	45.4%
D_{BC} > 500 nm number	0.25%	0.21%	0.38%

Aging in the atmosphere, agglomeration of water-bound rBC particles and size selection during snow formation and deposition would also influence BC size distribution in snow (Schwarz et al., 2013). Postdepositional processes also influence BC distributions (Doherty et al., 2013), although this happens due to snow melt, which was very limited at the sampling site (~1 mm each melt layer and borehole temperature of −34°C at 12 m depth). Other postdepositional processes such as agglomeration of BC via impaction of snowflakes or wind remobilization are unlikely without the presence of melt, due to the extreme volume dilution of BC in the snow (Schwarz et al., 2013).

The NMD observed in the Antarctic samples in this work (<80 nm) is similar to the NMD observed in Greenland snow (~90 nm—Mori

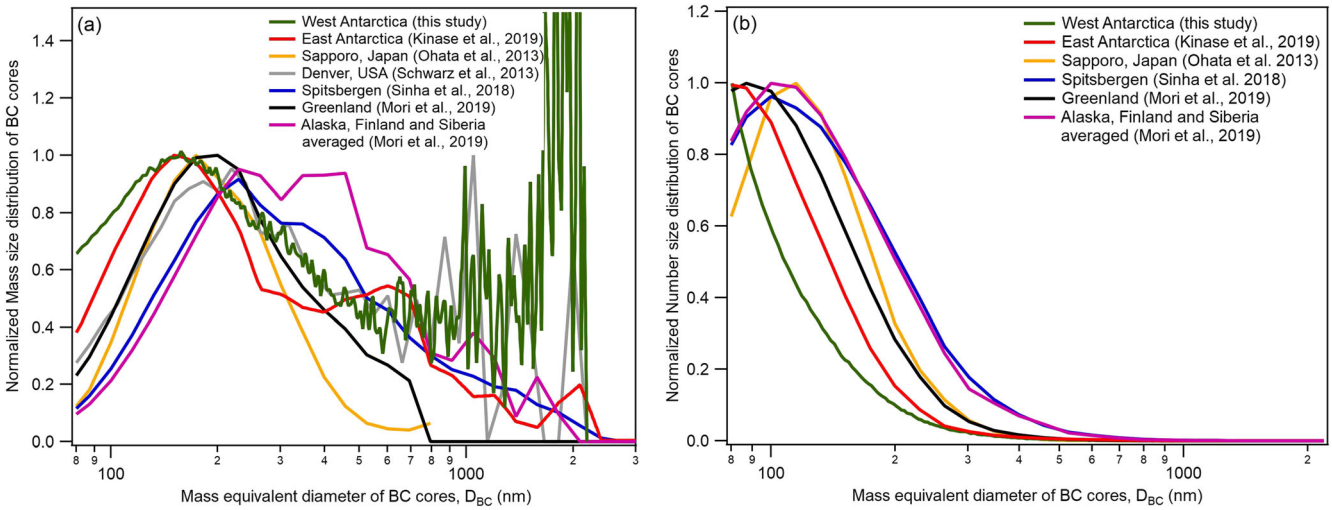

Figure 5. (a) Mass size distribution and (b) number distribution in snow from this work in comparison to previous studies in snow. Data were normalized to the finer mode peak (maximum *y*-value at the median size of the finer mode). Data from Alaska, Finland, and Siberia (Mori et al., 2019) were averaged together to maintain figure readability (results were similar to each other). Data from this work were normalized to the peak value of the finer mode maximum *y*-value (162 nm).

et al., 2019) and in East Antarctica (~70 nm—Kinase et al., 2019). This is also in agreement to previous qualitative observations that found abundant small rBC spherules with D_{BC} ~ 30 nm in Antarctic snow and ice (Ellis et al., 2016). An NMD in the Aitken mode (less than 100 nm diameter) is commonly related to fresh, high temperature BC emissions, originated from efficient fuel burning (Bond et al., 2013), although we consider unlikely that this NMD is related to fossil-fuel combustion or to fresh emissions. The sampling site is a remote place, with no nearby anthropogenic activity and air masses arriving at it underwent significant aging (Stohl & Sodemann, 2010). Also, previous works (Arienzo et al., 2017; Bisiaux, Edwards, McConnell, Albert, et al., 2012; Koch et al., 2007; Stohl & Sodemann, 2010) stated that BC in Antarctica mostly reflects long-range transport of biomass burning emissions from South America and Australia. At last, Ellis et al. (2016) observed these small BC spherules with D_{BC} ~ 30 nm in Antarctic ice dated to the year 1759 CE (before industrialization), which cannot reflect fossil fuel emissions. They did not observe discernable differences in BC morphology and sizes between the different time periods studied (preindustrialization and postindustrialization), which also corroborates that biomass burning is the likely origin.

Thus, long-range transport and aging of rBC particles in the atmosphere might be the dominant factors affecting the snow size distribution presented in this work. Kinase et al. (2019) found a similar MMD

Table 2
Size Distribution in Snow (MMD and NMD) From Different Parts of the Globe and Related References

Location	Reference	Number of samples	Type of sample	Primary MMD (nm)	Secondary MMDs (nm)	NMD (nm)
West Antarctica	This work	1,004	Snow/firn core	162 ± 40	673/1,040/1,810[a]	<80
West Antarctica	Khan et al. (2018)	11	Snowpit	300–400	-	-
East Antarctica	Kinase et al. (2019)	26	Surface snow	140	690	<80
Sapporo, Japan	Ohata et al. (2013)	20	Surface snow	175	-	115
Denver, USA	Schwarz et al. (2013)	5	Surface snow	220	-	-
Ny-Ålesund, Spitsbergen	Sinha et al. (2018)	167	Fresh snow, falling snow, and snowpack	240	-	102
Finland	Mori et al. (2019)	11	Snowpack and surface snow	358	-	110
Greenland	Mori et al. (2019)	68	Snowpack and surface snow	200	-	90
Alaska	Mori et al. (2019)	182	Snowpack and surface snow	320	1,200–1,400	100
Siberia	Mori et al. (2019)	29	Snowpack and surface snow	300	-	105

[a]Uncontained mode; see text.

(140 nm vs. 162 nm in this work) and attributed it to these factors, considering that larger rBC particles are removed more easily from the atmosphere than smaller ones during transport from source regions to Antarctica. The removal of large rBC particles from the atmosphere would also reflect minimal presence of large particles (>1,000 nm) in Antarctic snow, which is observed in this work.

Nevertheless, a few large particles were still present in the samples. As we observed that postdepositional processes that could affect rBC size distributions were very limited in the sampling site (e.g., melting), we suppose these few large particles may be a result of processes acting during snow formation in the atmosphere or during snow deposition. Unfortunately, rBC atmospheric measurements done so far are mostly up to 900 nm volume equivalent diameter (Cheng et al., 2018; Huang et al., 2011; Wang et al., 2014; Wu et al., 2017), and we do not have any measurements of the atmosphere at the drilling site to compare both atmospheric and snow size distributions.

Another supposition is that the large particles could be the remainders of long-range transport that removed most large rBC particles from the atmosphere but not all. Long-range transport of large particles generated in the atmosphere far away from Antarctica has been suggested by Ellis et al. (2016), which is not unreasonable considering mineral dust up to 5,000 nm can be transported over long distances (Gaiero et al., 2007; Mahowald et al., 2014) and be deposited in Antarctic snow (Delmonte et al., 2013; Li et al., 2008). Dust up to 2,400 nm has been found at the sampling site, associated with remote continental sources (e.g., South America—Cataldo et al., 2013; Schwanck et al., 2017), suggesting that large BC particles could also be transported this far. Further studies on rBC transport and deposition in snow, along with rBC size distributions from the atmosphere above it, would be of extreme value to improve our understanding in BC deposition in Antarctica.

5. Conclusions

Measurements of rBC size distributions in snow are important to adequately model BC impacts on the cryosphere but are still scarce. In this work we presented an rBC size distribution obtained from a 20 m deep snow/firn core from West Antarctica (1,004 melted samples). Results show a multimodal size distribution with a primary MMD of 162 ± 40 nm and secondary modes at 673 ± 48 and 1,040 ± 88, with slight seasonal differences (dry season MMD: 160 ± 40 nm; wet season MMD: 187 ± 31 nm). We observed a larger mode at ~1,810 nm but believe it is not fully characterized and in fact extends further than 2,000 nm. Our results are similar to recently published literature about East Antarctica rBC size distributions (Kinase et al., 2019) that found a primary MMD of ~140 nm, although one secondary mode observed in this study is similar to the one observed in Kinase et al. (2019) (~673 nm vs. ~690 nm, respectively). We consider postdepositional processes to have negligible influence to rBC size distribution due to very limited melt and to the extreme volume dilution of BC in the snow. Small particles (80 nm < D_{BC} < 100 nm) are abundant, accounting for 45.4% of all rBC cores detected by the SP2 but do not add significantly to rBC total mass (7.4%). Large particles (500 nm > D_{BC} > 2,000 nm) are very rare (0.25%) but represent a large portion of rBC total mass (36.4%). Contribution of particles with D_{BC} > 500 nm was higher in the wet season (mass: 45.4%, number: 0.38%) than in the dry season (mass: 33.3%, number: 0.21%). Dry season concentrations are 3.4 and 2 times that of the wet season in the ranges of 80 nm < D_{BC} < 500 nm (small particles) and 500 nm < D_{BC} < 2,000 nm (large particles), respectively; particle abundance in the dry season is 3.5 and 2 times that of the wet season for the same size ranges. These results corroborate the findings by Schwarz et al. (2013) that snow size distribution presents a significant contribution of larger particles to total rBC mass, much larger than atmospheric rBC size distributions. Also, our results indicate that large particles exist in Antarctic snow and ice and that despite their low occurrence, they can represent an important fraction of total rBC mass in the snow. More research comparing rBC size distributions in snow and in the air above it would be of great value to improve the understanding of rBC deposition in snow and the role of aging and snow formation processes to size distributions.

Conflict of Interest

The authors declare no conflict of interests of any kind.

Data Availability Statement

rBC size distribution data have been published online on PANGAEA repository as Marquetto, Kaspari, & Simões (2020): Refractory black carbon mass and number size distributions in West Antarctica snow and firn samples, PANGAEA (https://doi.org/10.1594/PANGAEA.920981).

Acknowledgments
This research is part of the Brazilian Antarctic Program (PROANTAR) and was financed with funds from the Brazilian National Council for Scientific and Technological Development (CNPq) Split Fellowship Program (no. 200386/2018-2), from the CNPq projects 465680/2014-3 and 442761/2018-0, CAPES project "INCT da Criosfera" 88887.136384/2017-00, and PROANTAR project 88887.314450/2019-00. We thank the Centro Polar e Climático (CPC/UFRGS) and the Department of Geological Sciences (CWU) faculty and staff for supporting this work. We also thank authors of Khan et al. (2018), Kinase et al. (2019), Ohata et al. (2013), Schwarz et al. (2013), Sinha et al. (2018), and Mori et al. (2019) for data availability and Joshua Schwarz and the two anonymous referees for their expertise and helpful suggestions. We also thank Martin Gysel, Anja Eicher, and Theo Jenk for their comments on internal calibration of the SP2 for snow samples.

References

Arienzo, M. M., McConnell, J. R., Murphy, L. N., Chellman, N., Das, S., Kipfstuhl, S., & Mulvaney, R. (2017). Holocene black carbon in Antarctica paralleled Southern Hemisphere climate. *Journal of Geophysical Research: Atmospheres*, *122*, 6713–6728. https://doi.org/10.1002/2017JD026599

Baumgardner, D., Popovicheva, O., Allan, J., Bernardoni, V., Cao, J., Cavalli, F., et al. (2012). Soot reference materials for instrument calibration and intercomparisons: A workshop summary with recommendations. *Atmospheric Measurement Techniques*, *5*(8), 1869–1887. https://doi.org/10.5194/amt-5-1869-2012

Bice, K., Eil, A., Habib, B., Heijmans, P., Kopp, R., Nogues, J., et al. (2009). Black carbon: A review and policy recommendations. In *Woodrow Wilson School of Public and International Affairs*. Princeton, NJ: EUA.

Bisiaux, M. M., Edwards, R., McConnell, J. R., Albert, M. R., Anschütz, H., Neumann, T. A., et al. (2012). Variability of black carbon deposition to the East Antarctic Plateau, 1800-2000 AD. *Atmospheric Chemistry and Physics*, *12*(8), 3799–3808. https://doi.org/10.5194/acp-12-3799-2012

Bisiaux, M. M., Edwards, R., McConnell, J. R., Curran, M. a. J., Van Ommen, T. D., Smith, A. M., et al. (2012). Changes in black carbon deposition to Antarctica from two high-resolution ice core records, 1850-2000 AD. *Atmospheric Chemistry and Physics*, *12*(9), 4107–4115. https://doi.org/10.5194/acp-12-4107-2012

Bond, T. C., Doherty, S. J., Fahey, D. W., Forster, P. M., Berntsen, T., Deangelo, B. J., et al. (2013). Bounding the role of black carbon in the climate system: A scientific assessment. *Journal of Geophysical Research: Atmospheres*, *118*, 5380–5552. https://doi.org/10.1002/jgrd.50171

Casey, K. A., Kaspari, S. D., Skiles, S. M., Kreutz, K., & Handley, M. J. (2017). The spectral and chemical measurement of pollutants on snow near South Pole, Antarctica. *Journal of Geophysical Research: Atmospheres*, *122*, 6592–6610. https://doi.org/10.1002/2016JD026418

Cataldo, M., Evangelista, H., Simões, J. C., Godoi, R. H. M., Simmonds, I., Hollanda, M. H., et al. (2013). Mineral dust variability in central West Antarctica associated with ozone depletion. *Atmospheric Chemistry and Physics*, *13*, 2165–2175. https://doi.org/10.5194/acp-13-2165-2013

Cheng, Y., Li, S. M., Gordon, M., & Liu, P. (2018). Size distribution and coating thickness of black carbon from the Canadian oil sands operations. *Atmospheric Chemistry and Physics*, *18*, 2653–2667. https://doi.org/10.5194/acp-18-2653-2018

Delaney, I., Kaspari, S., & Jenkins, M. (2015). Black carbon concentrations in snow at Tronsen Meadow in Central Washington from 2012 to 2013: Temporal and spatial variations and the role of local forest fire activity. *Journal of Geophysical Research: Atmospheres*, *120*, 9160–9172. https://doi.org/10.1002/2017JD027560

Delmonte, B., Baroni, C., Andersson, P. S., Narcisi, B., Salvatore, M. C., Petit, J. R., et al. (2013). Modern and Holocene aeolian dust variability from Talos Dome (Northern Victoria Land) to the interior of the Antarctic ice sheet. *Quaternary Science Reviews*, *64*, 76–89. https://doi.org/10.1016/j.quascirev.2012.11.033

Doherty, S. J., Grenfell, T. C., Forsström, S., Hegg, D. L., Brandt, R. E., & Warren, S. G. (2013). Observed vertical redistribution of black carbon and other insoluble light-absorbing particles in melting snow. *Journal of Geophysical Research: Atmospheres*, *118*, 5553–5569. https://doi.org/10.1002/jgrd.50235

Droplet Measurement Technologies (2013a). *PSI Toolkit for the Single Particle Soot Manual—DOC-0359 Revision A*. Boulder, CO: Droplet Measurement Technologies.

Droplet Measurement Technologies (2013b). Single Particle Soot Photometer (SP2) Operator Manual.

Ellis, A., Edwards, R., Saunders, M., Chakrabarty, R. K., Subramanian, R., Timms, N. E., et al. (2016). Individual particle morphology, coatings, and impurities of black carbon aerosols in Antarctic ice and tropical rainfall. *Geophysical Research Letters*, *43*, 11,875–11,883. https://doi.org/10.1002/2016GL071042

Flanner, M. G., Zender, C. S., Randerson, J. T., & Rasch, P. J. (2007). Present-day climate forcing and response from black carbon in snow. *Journal of Geophysical Research*, *112*, D11202. https://doi.org/10.1029/2006JD008003

Fretwell, P., Pritchard, H. D., Vaughan, D. G., Bamber, J. L., Barrand, N. E., Bell, R., et al. (2013). Bedmap2: Improved ice bed, surface and thickness datasets for Antarctica. *The Cryosphere*, *7*, 375–393. https://doi.org/10.5194/tc-7-375-2013

Gaiero, D. M., Brunet, F., Probst, J. L., & Depetris, P. J. (2007). A uniform isotopic and chemical signature of dust exported from Patagonia: Rock sources and occurrence in southern environments. *Chemical Geology*, *238*(1–2), 107–120. https://doi.org/10.1016/j.chemgeo.2006.11.003

Goldberg, E. D. (1985). *Black carbon in the environment* (1st ed.). New York: Wiley.

Gysel, M., Laborde, M., Olfert, J. S., Subramanian, R., & Gréhn, A. J. (2011). Effective density of Aquadag and fullerene soot black carbon reference materials used for SP2 calibration. *Atmospheric Measurement Techniques*, *4*(12), 2851–2858. https://doi.org/10.5194/amt-4-2851-2011

Hadley, O. L., & Kirchstetter, T. W. (2012). Black-carbon reduction of snow albedo. *Nature Climate Change*, *2*(6), 437–440. https://doi.org/10.1038/nclimate1433

Hansen, J., & Nazarenko, L. (2004). Soot climate forcing via snow and ice albedos. *Proceedings of the National Academy of Sciences of the United States of America*, *101*(2), 423–428. https://doi.org/10.1073/pnas.2237157100

He, C., Liou, K. N., & Takano, Y. (2018). Resolving size distribution of black carbon internally mixed with snow: Impact on snow optical properties and albedo. *Geophysical Research Letters*, *45*, 2697–2705. https://doi.org/10.1002/2018GL077062

Huang, X. F., Gao, R. S., Schwarz, J. P., He, L. Y., Fahey, D. W., Watts, L. A., et al. (2011). Black carbon measurements in the Pearl River Delta region of China. *Journal of Geophysical Research*, *116*, D12208. https://doi.org/10.1029/2010JD014933

IPCC (2013). In V. B. & P. M. M, T. F. Stocker, et al. (Eds.), *Climate Change 2013: Climate Change 2013: The Physical Science Basis. Contribution of Working Group I to the Fifth Assessment Report of the Intergovernmental Panel on Climate Change* (Vol. 5). Cambridge and New York: Cambridge University Press.

Kaspari, S., Painter, T. H., Gysel, M., Skiles, S. M., & Schwikowski, M. (2014). Seasonal and elevational variations of black carbon and dust in snow and ice in the Solu-Khumbu, Nepal and estimated radiative forcings. *Atmospheric Chemistry and Physics*, *14*, 8089–8103. https://doi.org/10.5194/acp-14-8089-2014

Kaspari, S. D., Schwikowski, M., Gysel, M., Flanner, M. G., Kang, S., Hou, S., & Mayewski, P. A. (2011). Recent increase in black carbon concentrations from a Mt. Everest ice core spanning 1860-2000 AD. *Geophysical Research Letters*, *38*, L04703. https://doi.org/10.1029/2010GL046096

Katich, J. M., Perring, A. E., & Schwarz, J. P. (2017). Optimized detection of particulates from liquid samples in the aerosol phase: Focus on black carbon. *Aerosol Science and Technology*, *51*, 543–553. https://doi.org/10.1080/02786826.2017.1280597

Khan, A. L., McMeeking, G. R., Schwarz, J. P., Xian, P., Welch, K. A., Berry Lyons, W., & McKnight, D. M. (2018). Near-surface refractory black carbon observations in the atmosphere and snow in the McMurdo dry valleys, Antarctica, and potential impacts of Foehn winds. *Journal of Geophysical Research: Atmospheres*, *123*, 2877–2887. https://doi.org/10.1002/2017JD027696

Kinase, T., Adachi, K., Oshima, N., Goto-Azuma, K., Ogawa-Tsukagawa, Y., Kondo, Y., et al. (2019). Concentrations and size distributions of black carbon in the surface snow of Eastern Antarctica in 2011. *Journal of Geophysical Research: Atmospheres*, *125*, 2019JD030737. https://doi.org/10.1029/2019JD030737

Koch, D., Bond, T. C., Streets, D., Unger, N., & van der Werf, G. R. (2007). Global impacts of aerosols from particular source regions and sectors. *Journal of Geophysical Research*, *112*, D02205. https://doi.org/10.1029/2005JD007024

Legrand, M., & Mayewski, P. (1997). Glaciochemistry of polar ice cores: A review. *Reviews of Geophysics*, *35*(3), 219–243. https://doi.org/10.1029/96RG03527

Li, F., Ginoux, P., & Ramaswamy, V. (2008). Distribution, transport, and deposition of mineral dust in the Southern Ocean and Antarctica: Contribution of major sources. *Journal of Geophysical Research*, *113*, D10207. https://doi.org/10.1029/2007JD009190

Lim, S., Faïn, X., Ginot, P., Mikhalenko, V., Kutuzov, S., Paris, J., et al. (2017). Black carbon variability since preindustrial times in the eastern part of Europe reconstructed from Mt. Elbrus, Caucasus, ice cores. *Atmospheric Chemistry and Physics*, *17*, 3489–3505. https://doi.org/10.5194/acp-17-3489-2017

Lim, S., Faïn, X., Zanatta, M., Cozic, J., Jaffrezo, J.-L., Ginot, P., & Laj, P. (2014). Refractory black carbon mass concentrations in snow and ice: Method evaluation and inter-comparison with elemental carbon measurement. *Atmospheric Measurement Techniques*, *7*, 3307–3324. https://doi.org/10.5194/amt-7-3307-2014

Mahowald, N., Albani, S., Kok, J. F., Engelstaeder, S., Scanza, R., Ward, D. S., & Flanner, M. G. (2014). The size distribution of desert dust aerosols and its impact on the Earth system. *Aeolian Research*, *15*, 53–71. https://doi.org/10.1016/j.aeolia.2013.09.002

Marquetto, L., Kaspari, S., & Simões, J. C. (2020). Refractory black carbon (rBC) variability in a 47-year West Antarctic snow and firn core. *The Cryosphere*, *14*, 1537–1554. https://doi.org/10.5194/tc-14-1537-2020

Marquetto, L., Kaspari, S., Simões, J. C., & Babik, E. (2020). Refractory black carbon results and a method comparison between solid-state cutting and continuous melting sampling of a West Antarctic snow and firn core. *Advances in Atmospheric Sciences*, *37*, 1–10. https://doi.org/10.1007/s00376-019-9124-8

McConnell, J. R., Edwards, R., Kok, G. L., Flanner, M. G., Zender, C. S., Saltzman, E. S., et al. (2007). 20th-century industrial black carbon emissions altered Arctic climate forcing. *Science*, *317*(5843), 1381–1384. https://doi.org/10.1126/science.1144856

Mori, T., Goto-Azuma, K., Kondo, Y., Ogawa-Tsukagawa, Y., Miura, K., Hirabayashi, M., et al. (2019). Black carbon and inorganic aerosols in Arctic snowpack. *Journal of Geophysical Research: Atmospheres*, *124*, 2019JD030623. https://doi.org/10.1029/2019JD030623

Mori, T., Kondo, Y., Ohata, S., Moteki, N., Matsui, H., Oshima, N., & Iwasaki, A. (2014). Wet deposition of black carbon at a remote site in the East China Sea. *Journal of Geophysical Research: Atmospheres*, *119*, 10,485–10,498. https://doi.org/10.1002/2014JD022103

Mori, T., Moteki, N., Ohata, S., Koike, M., Goto-Azuma, K., Miyazaki, Y., & Kondo, Y. (2016). Improved technique for measuring the size distribution of black carbon particles in liquid water. *Aerosol Science and Technology*, *50*, 242–254. https://doi.org/10.1080/02786826.2016.1147644

Moteki, N., & Kondo, Y. (2010). Dependence of laser-induced incandescence on physical properties of black carbon aerosols: Measurements and theoretical interpretation. *Aerosol Science and Technology*, *44*(8), 663–675. https://doi.org/10.1080/02786826.2010.484450

Moteki, N., Kondo, Y., Takegawa, N., & Nakamura, S. I. (2009). Directional dependence of thermal emission from nonspherical carbon particles. *Journal of Aerosol Science*, *40*(9), 790–801. https://doi.org/10.1016/j.jaerosci.2009.05.003

Neff, P. D., & Bertler, N. A. N. (2015). Trajectory modeling of modern dust transport to the Southern Ocean and Antarctica. *Journal of Geophysical Research: Atmospheres*, *120*, 9303–9322. https://doi.org/10.1002/2015JD023304

Ohata, S., Moteki, N., Schwarz, J. P., Fahey, D. W., & Kondo, Y. (2013). Evaluation of a method to measure black carbon particles suspended in rainwater and snow samples. *Aerosol Science and Technology*, *47*, 1073–1082. https://doi.org/10.1080/02786826.2013.824067

Olfert, J. S., & Collings, N. (2005). New method for particle mass classification—The Couette centrifugal particle mass analyzer. *Journal of Aerosol Science*, *36*(11), 1338–1352. https://doi.org/10.1016/j.jaerosci.2005.03.006

Osmont, D., Sigl, M., Eichler, A., Jenk, T. M., & Schwikowski, M. (2019). A Holocene black carbon ice-core record of biomass burning in the Amazon Basin from Illimani, Bolivia. *Climate of the Past*, *15*, 579–592. https://doi.org/10.5194/cp-15-579-2019

Osmont, D., Wendl, I. A., Schmidely, L., Sigl, M., Vega, C. P., Isaksson, E., & Schwikowski, M. (2018). An 800-year high-resolution black carbon ice core record from Lomonosovfonna, Svalbard. *Atmospheric Chemistry and Physics*, *18*, 12,777–12,795. https://doi.org/10.5194/acp-18-12777-2018

Petzold, A., Ogren, J. A., Fiebig, M., Laj, P., Li, S. M., Baltensperger, U., et al. (2013). Recommendations for reporting black carbon measurements. *Atmospheric Chemistry and Physics*, *13*, 8365–8379. https://doi.org/10.5194/acp-13-8365-2013

Reid, J. S., Koppmann, R., Eck, T. F., & Eleuterio, D. P. (2005). A review of biomass burning emissions part II: Intensive physical properties of biomass burning particles. *Atmospheric Chemistry and Physics*, *5*(3), 799–825. https://doi.org/10.5194/acp-5-799-2005

Sand, M., Samset, B. H., Balkanski, Y., Bauer, S., Bellouin, N., Berntsen, T. K., et al. (2017). Aerosols at the poles: An AeroCom Phase II multi-model evaluation. *Atmospheric Chemistry and Physics*, *17*, 12,197–12,218. https://doi.org/10.5194/acp-17-12197-2017

Schwanck, F., Simões, J. C., Handley, M., Mayewski, P. A., Auger, J. D., Bernardo, R. T., & Aquino, F. E. (2017). A 125-year record of climate and chemistry variability at the Pine Island Glacier ice divide, Antarctica. *The Cryosphere*, *11*, 1537–1552. https://doi.org/10.5194/tc-11-1537-2017

Schwarz, J. P., Doherty, S. J., Li, F., Ruggiero, S. T., Tanner, C. E., Perring, A. E., et al. (2012). Assessing single particle soot photometer and integrating sphere/integrating sandwich spectrophotometer measurement techniques for quantifying black carbon concentration in snow. *Atmospheric Measurement Techniques*, *5*(11), 2581–2592. https://doi.org/10.5194/amt-5-2581-2012

Schwarz, J. P., Gao, R. S., Fahey, D. W., Thomson, D. S., Watts, L. A., Wilson, J. C., et al. (2006). Single-particle measurements of midlatitude black carbon and light-scattering aerosols from the boundary layer to the lower stratosphere. *Journal of Geophysical Research*, *111*, D16207. https://doi.org/10.1029/2006JD007076

Schwarz, J. P., Gao, R. S., Perring, A. E., Spackman, J. R., & Fahey, D. W. (2013). Black carbon aerosol size in snow. *Nature Scientific Reports*, *3*, 1356. https://doi.org/10.1038/srep01356

Schwarz, J. P., Spackman, J. R., Gao, R. S., Perring, A. E., Cross, E., Onasch, T. B., et al. (2010). The detection efficiency of the single particle soot photometer. *Aerosol Science and Technology*, *44*(8), 612–628. https://doi.org/10.1080/02786826.2010.481298

Sigl, M., Abram, N. J., Gabrieli, J., Jenk, T. M., Osmont, D., & Schwikowski, M. (2018). 19th century glacier retreat in the Alps preceded the emergence of industrial black carbon deposition on high-alpine glaciers. *The Cryosphere*, *12*, 3311–3331. https://doi.org/10.5194/tc-12-3311-2018

Sinclair, K. E., Bertler, N. A. N., & Trompetter, W. J. (2010). Synoptic controls on precipitation pathways and snow delivery to high-accumulation ice core sites in the Ross Sea region, Antarctica. *Journal of Geophysical Research*, *115*, D22112. https://doi.org/10.1029/2010JD014383

Sinha, P. R., Kondo, Y., Goto-Azuma, K., Tsukagawa, Y., Fukuda, K., Koike, M., et al. (2018). Seasonal progression of the deposition of black carbon by snowfall at Ny-Ålesund, Spitsbergen. *Journal of Geophysical Research: Atmospheres*, *123*, 997–1016. https://doi.org/10.1002/2017JD028027

Slowik, J. G., Cross, E. S., Han, J.-H., Davidovits, P., Onasch, T. B., Jayne, J. T., et al. (2007). An inter-comparison of instruments measuring black carbon content of soot particles. *Aerosol Science and Technology*, *41*(3), 295–314. https://doi.org/10.1080/02786820701197078

Stohl, A., & Sodemann, H. (2010). Characteristics of atmospheric transport into the Antarctic troposphere. *Journal of Geophysical Research*, *115*, D02305. https://doi.org/10.1029/2009JD012536

Symonds, J. P. R., Reavell, K. S. J., & Olfert, J. S. (2013). The CPMA-electrometer system—A suspended particle mass concentration standard. *Aerosol Science and Technology*, *47*, i–iv. https://doi.org/10.1080/02786826.2013.801547

Thevenon, F., Anselmetti, F. S., Bernasconi, S. M., & Schwikowski, M. (2009). Mineral dust and elemental black carbon records from an Alpine ice core (Colle Gnifetti glacier) over the last millennium. *Journal of Geophysical Research*, *114*, D17102. https://doi.org/10.1029/2008JD011490

Wang, Q., Schwarz, J. P., Cao, J., Gao, R., Fahey, D. W., Hu, T., et al. (2014). Black carbon aerosol characterization in a remote area of Qinghai-Tibetan plateau, western China. *Science of the Total Environment*, *479–480*, 151–158. https://doi.org/10.1016/j.scitotenv.2014.01.098

Warren, S. G., & Wiscombe, W. J. (1980). A model for spectral albedo of snow II: Snow containing atmospheric aerosols. *Journal of the Atmospheric Sciences*, *37*(12), 2734–2745. https://doi.org/10.1175/1520-0469(1980)037<2734:AMFTSA>2.0.CO;2

Wendl, I. A., Menking, J. A., Färber, R., Gysel, M., Kaspari, S. D., Laborde, M. J. G., & Schwikowski, M. (2014). Optimized method for black carbon analysis in ice and snow using the single particle soot photometer. *Atmospheric Measurement Techniques*, *7*, 2667–2681. https://doi.org/10.5194/amt-7-2667-2014

Winstrup, M., Vallelonga, P., Kjær, H. A., Fudge, T. J., Lee, J. E., Riis, M. H., et al. (2019). A 2700-year annual timescale and accumulation history for an ice core from Roosevelt Island, West Antarctica. *Climate of the Past*, *15*, 751–779. https://doi.org/10.5194/cp-15-751-2019

Wu, Y., Wang, X., Tao, J., Huang, R., Tian, P., Cao, J., et al. (2017). Size distribution and source of black carbon aerosol in urban Beijing during winter haze episodes. *Atmospheric Chemistry and Physics*, *17*, 7965–7975. https://doi.org/10.5194/acp-17-7965-2017